SLAC-PUB-4179
December 1986
(M)

UNIQUE RADIATION PROBLEMS ASSOCIATED WITH THE SLAC LINEAR COLLIDER*

T. M. JENKINS and W. R. NELSON

Stanford Linear Accelerator Center
Stanford University, Stanford, California 94305

ABSTRACT

The SLAC Linear Collider (SLC) is a variation of a new class of colliders whereby two linear accelerators are aimed at each other to collide intense bunches of electrons and positrons together. Conventional storage rings are becoming ever more costly as the energy of the stored beams increases such that the cost of two linear colliders per GeV is less than that of electron-positron storage rings at c.m. energies above about 100 GeV. The SLC being built at SLAC is designed to achieve a center-of-mass energy of 100 GeV by accelerating intense bunches of particles, both electrons and positrons, in the SLAC linac and transporting them along two different arcs to a point where they're focused to a small radius and made to collide head on. The SLC has two main goals. The first is to develop the physics and technology of linear colliders. The other is to achieve center-of-mass energies above 90 GeV in order to investigate the unification of the weak and electromagnetic interactions in the energy range above 90 GeV; (*i.e.*, Z^o, etc.).

This note discusses a few of the special problems that were encountered by the Radiation Physics group at SLAC during the design and construction of the SLAC Linear Collider. The nature of these problems is discussed along with the methods employed to solve them.

INTRODUCTION

True linear colliders, of which SLC is a variant, can tolerate extremely high current densities at the collision point compared to storage rings because the beam is subsequently thrown away. Thus, any disruptions of the beam through beam-beam interactions don't affect the next collision in a linear collider whereas they would blow the beam up in a storage ring. Also, since a linear collider doesn't store particles in a ring of magnets, it doesn't require the large amounts of rf power to make up for synchrotron losses that occur in storage rings. These two factors combine to reduce the cost of linear colliders versus storage rings; the cost of storage rings scales roughly as the square of the center-of-mass energy whereas the cost of a linear collider scales as the first power of the energy.

While the SLC does have a ring of magnets to bring the beams to the collision point, at energies below about 70 GeV per beam the synchrotron radiation emitted has negligible effect on the total power to run the facility.

* Work supported by the Department of Energy, contract DE – AC03 – 76SF00515.
Invited talk at the Midyear Symposium of the Health Physics Society, Reno, Nevada, Feb. 8-12, 1987

A schematic of the complete system is shown in Fig. 1.

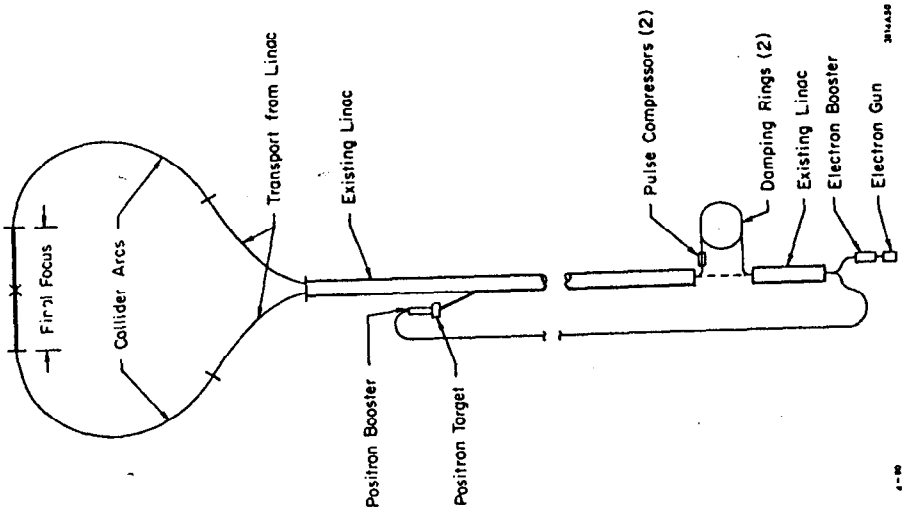

Figure 1. General layout of the SLAC Linear Collider.

The SLC is designed to operate with a luminosity of $6.0 \times 10^{30}\text{cm}^{-2}\text{sec}^{-1}$ (1). Very simply, luminosityis a function of the number of particles in each bunch, the rep rate and the inverse of the cross sectional area of the two beams. To achieve the design criterion, the beam intensity will be 5×10^{10} particles per each bunch (e^+, e^-) and the beam radius at the interaction point will be about 2 microns. This small beam spot size will be achieved partly through the use of cooling of the beams in damping rings near the beginning of the linac, and partly through a pinch effect at the interaction point itself.

The cycle begins with two bunches of 5×10^{10} particles in each damping ring, each at an energy of 1.2 GeV. One of the positron bunches is extracted from the damping ring followed by both electron bunches from the other damping ring. Typical spacing between bunches is about 15 meters (*i.e.*, 50 nsec) in the linac.

The three bunches are then accelerated down the linac. At the two-thirds point, the trailing electron bunch is extracted from the linac and directed onto a positron-production target. The other electron and positron bunches continue to the end of the linac where they reach an energy of 51 GeV and are sent into the two arcs, losing about 1 GeV per bunch from synchrotron radiation in the process. After emerging from the arcs, the bunches pass through achromatic matching and focusing sections which focus the beams to very small sizes at the collision point.

Meanwhile, the positrons produced at the two-thirds point are accelerated to 200 MeV, bent through 180^o , sent back into the existing accelerator tunnel and then to the beginning of the linac. There, they are bent 180^o and reinjected into the first sector of the linac and the cycle begins anew.

A typical operation is shown in Fig. 2.

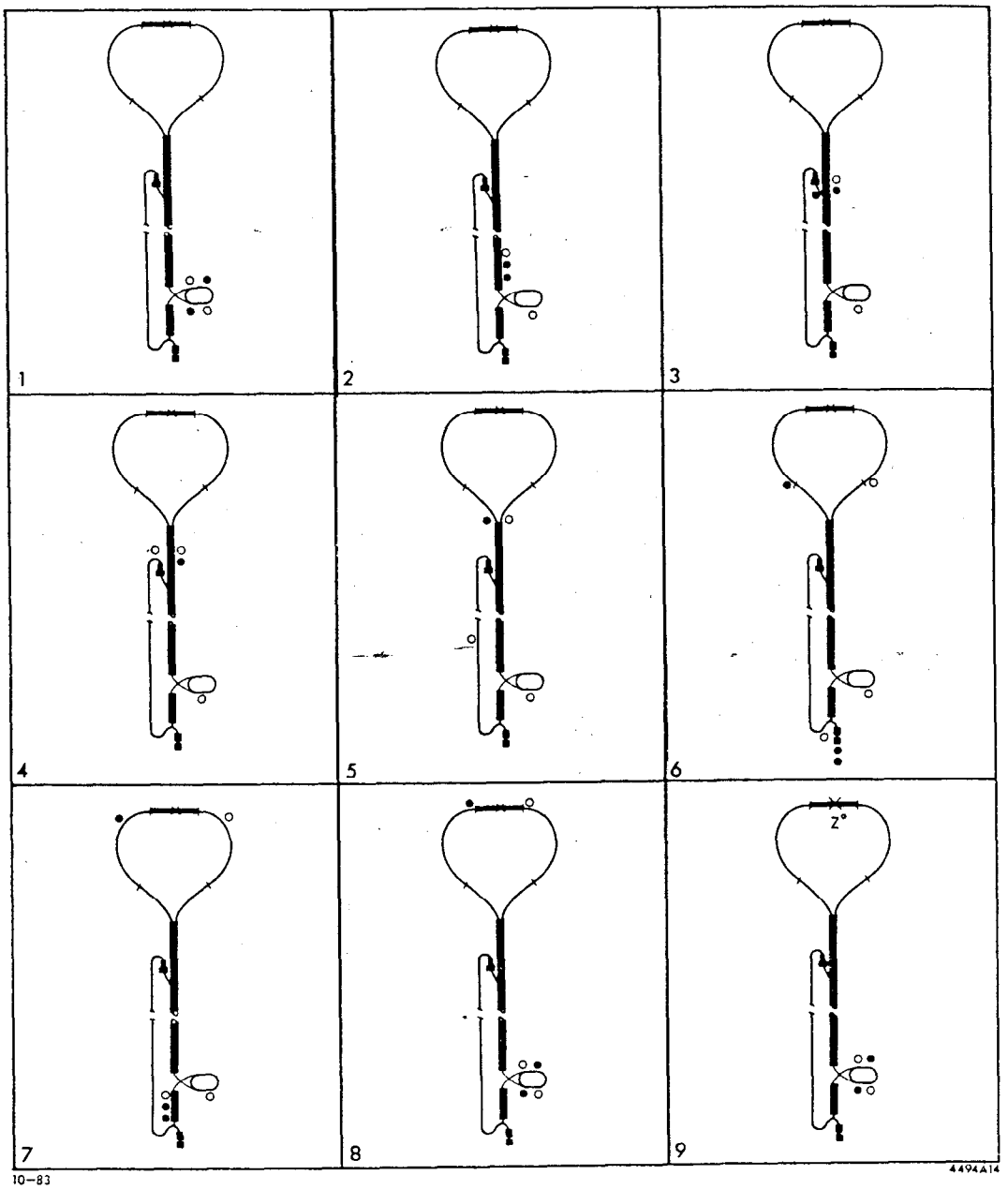

Figure 2. A typical operating cycle of the SLC showing electrons and positrons at different times in the operating cycle. Open circles = positrons; closed circles = electrons.

Because the emittance of the positron beam is very much larger than that required for collider operation, a positron bunch must remain in the damping ring for approximately four radiation damping times which corresponds to twice the time interval between linac pulses. Thus, the positron bunch to be used in the next linac cycle is the one that is still stored in the damping ring from the previous cycle.

Table 1 summarizes parameters important for radiation transport.

Table 1

Parameters of the SLC

Parameter	Interaction point	Arcs	Linac	Positron source	Damping rings
Energy	50 GeV	50 GeV	51 GeV	33 GeV	1.2 GeV
Luminosity	$6 \times 10^{30}\text{cm}^{-2}\text{sec}^{-1}$				
Rep Rate	180 Hz				
Bunch Length (IP)	1.0 mm				
Beam size ($\sigma_x = \sigma_y$)	1.65 microns				
Pinch factor	2.2				
Particles/bunch	5×10^{10}		5×10^{10}	5×10^{10}	5×10^{10}
Power	72 kW			47 kW	
Average radius		300 m			
Focusing Structure		AG			
Vacuum		$< 10^{-2}$ torr			
Bunch length			1 mm		
e^+ energy from tgt.				2-20 MeV	
Energy into linac				200 MeV	
Number of bunches					2
Damping time					2.9 ms

The task of shielding the SLC consists of parts which are simply extensions of previous shielding methods, and parts which are quite unique. The main linac is already underground, shielded many years ago for beam powers in excess of 1 MW. The SLC beam power in the linac, which consists of three bunches per pulse of 5×10^{10} electrons or positrons per bunch, could be as high as 144 kW at the 2/3 point (33 GeV and three bunches), 147 kW at the end of the linac (51 GeV and two bunches) and 144 kW at the interaction point if both bunches were to be absorbed at a machine rep rate of 180 pps. Therefore, no further shielding is needed for the main linac.

The SLC arcs, which are new, have been placed deep underground for reasons of economy of construction as well as the desire to eliminate any boundary doses. Care was taken in the shielding of the Collider Experimental Hall to avoid high dose rates for the accident situation (*e.g.*, a missteered beam), but for normal running, the needs of the physics detector for a low radiation background are much greater than people requirements. Still, for the most part, shielding calculations were traditional; *i.e.*, those based on previous methods (2-6).

The most unique problems, for which there is time to include only a sampling, aren't associated with radiation shielding *per se*, but with radiation transport. We note here that the job of the health physicist isn't tightly defined to include only personnel protection. There are times when other disciplines and that of health physics overlap, as in the case of patient dosimetry for medical radiation treatment, or when the accelerator designer or the research physicist needs radiation transport information in order to design his machine correctly. A good part of the radiation transport expertise rests within the health physics community. It's no accident that many of the most used radiation trans-

port codes come from within health physics groups: *e.g.* CASIM at Fermilab (7), EGS at SLAC (8), FLUKA at CERN (9), and HETC at ORNL (20). They were created to fulfill particle production and radiation transport needs and have remained with health physics ever since.

Fig. 3 is an elevation profile of the arcs showing the earth overburden.

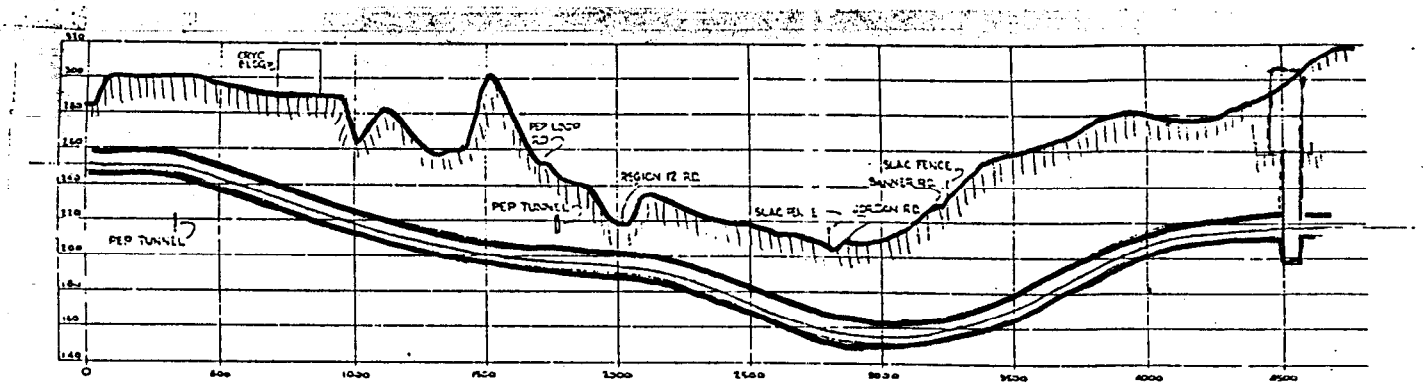

North Profile

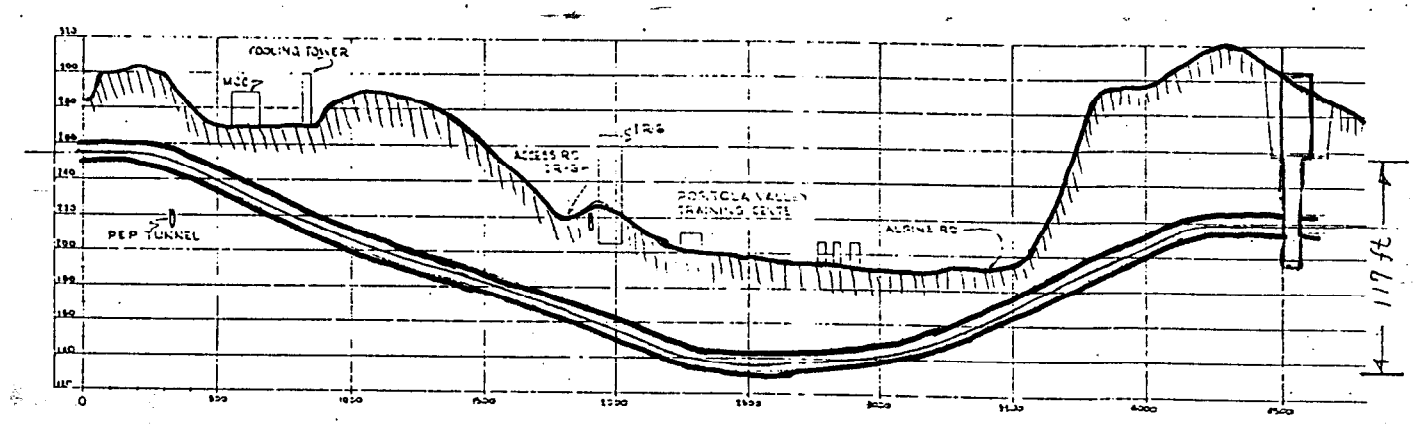

South Profile

Figure 3. Elevation profile of the arcs showing the earth overburden.

The requirements for high intensity and very small beam spot sizes pose special problems in radiation transport and in beam containment. These problems can be as diverse as 1) beam heating and burn-through, 2) ion chamber response and 3) radiation damage to electronics in the arc alcoves. We'll touch briefly on each of these topics.

ENERGY DEPOSITION AND BURN-THROUGH

Beams of 5×10^{10} electrons and 5×10^{10} positrons per bunch each with a diameter of about 50μ pose a considerable heat deposition problem. The danger of accidental damage to components is greater than previously encountered at SLAC. The design of beam dumps and protection collimators requires care in the choice of materials, and may necessitate the use of "spoilers" (*i.e.*, thin foils) to increase beam size.

Energy Deposition in Dumps and Beam Pipes

The first look at this problem (10) was done using the EGS3 (8) Monte Carlo code with improvements in subroutine CYLNDR to avoid problems at small radii due to truncation errors. EGS3 was run with zero emittance beams and with two quantities plotted. The first was the energy density divided by the incident beam energy, which is independent of beam intensity. The second quantity was the single pulse temperature rise for 5×10^{10} incident electrons. Then, in order to obtain similar results for finite size beams, the EGS3 output was folded with a two-dimensional Gaussian with standard deviations, $\sigma_x = \sigma_y = 50\mu$. This method proved acceptable, but was later replaced by one using the newer EGS4 code (11) and a 'leading particle' biasing scheme (see below).

A single 50 GeV shower generated by EGS4 in a 1 mm copper slab is shown in Fig. 4 (12).

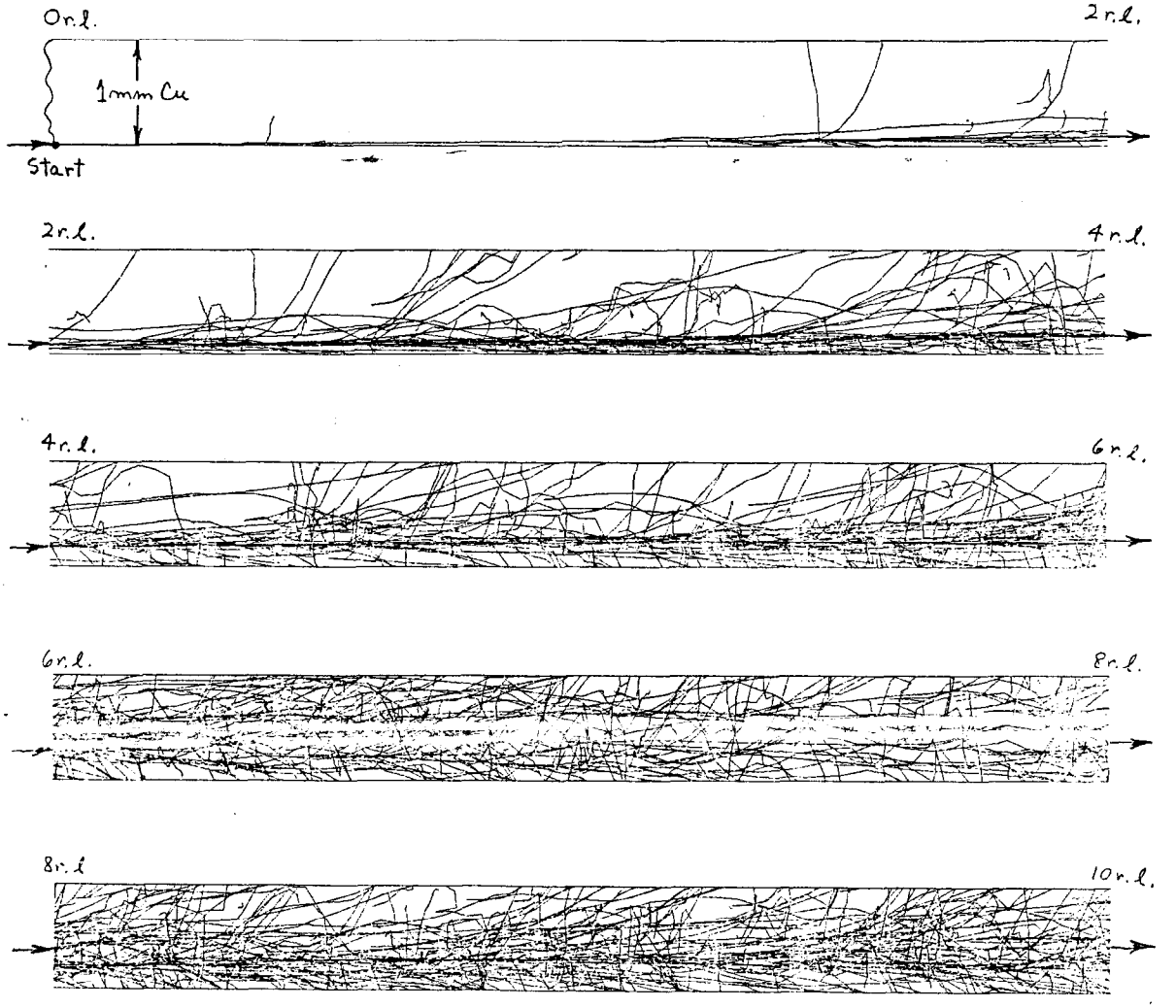

Figure 4. An electromagnetic cascade initiated in a 1 mm Cu slab by a single 50 GeV electron incident at a 3 mm glancing angle. To avoid confusion, only charged particle tracks inside the slab are shown. Note the "core" of the shower due to bremsstrahlung and pair production.

With EGS4, variance reduction techniques (*e.g.*, leading particle biasing) can be implemented in order to improve the efficiency for generating showers. The problem of heating occurs not only in dumps and collimators, but also in parts of the beam transport system which aren't supposed to intercept beam: *e.g.*, the beam pipe itself, beam position monitors, etc. Variance reduction techniques were found to be important for the problems of component heating since the beam spot needed to be sampled over a Gaussian distribution. For example, a typical 50 GeV shower event takes slightly less than one minute on the IBM-3081 using EGS4; consequently, very few samples could be taken over the beam spot in a reasonable time. With leading particle biasing however, we were able to generate between 1000 and 6000 showers per minute, depending on the material, slab thickness and angle of incidence. Since we know that the electromagnetic shower predominately involves bremsstrahlung and pair production interactions, and since high energy particles are the most influential, we should be able to speed up the calculation by forcing selection of the 'leading particle' — *i.e.*, the higher of two energies in any bremsstrahlung or pair production interaction — discarding the lower energy partner. To play the game fairly, one must randomly select the lower energy particle some of the time and assign an appropriate weight factor to the particle selected each time. Then instead of counting particles, we sum weights and also weight the energy deposition.

These EGS4 calculations were compared with the previous EGS3 calculations where the Gaussian spread of the beam was folded semi-analytically into the EGS results. The results were essentially identical everywhere except for a slight difference in the first radial bin.

Fig. 5 and Fig. 6 show the maximum energy deposition and temperature rise in 1 mm copper and aluminum slabs (12), respectively, with σ = 0.05 mm.

FIG.5: MAXIMUM E-DEPOSITION AND TEMPERATURE RISE FOR ELECTRON BEAMS WITH σ=0.05 MM

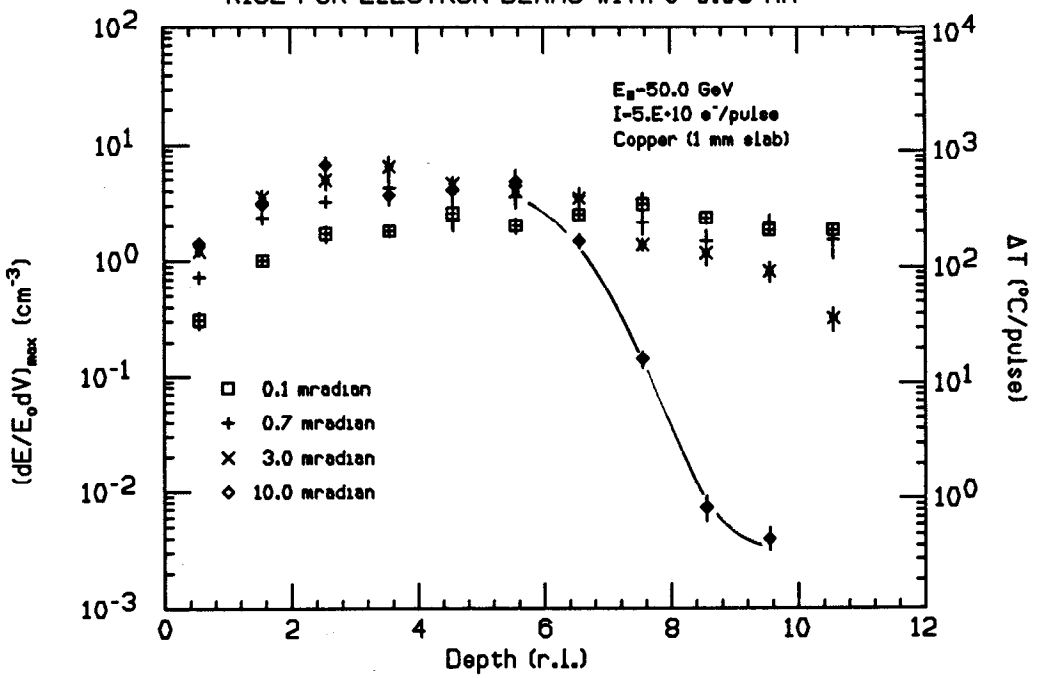

FIG.6: MAXIMUM E-DEPOSITION AND TEMPERATURE RISE FOR ELECTRON BEAMS WITH σ=0.05 MM

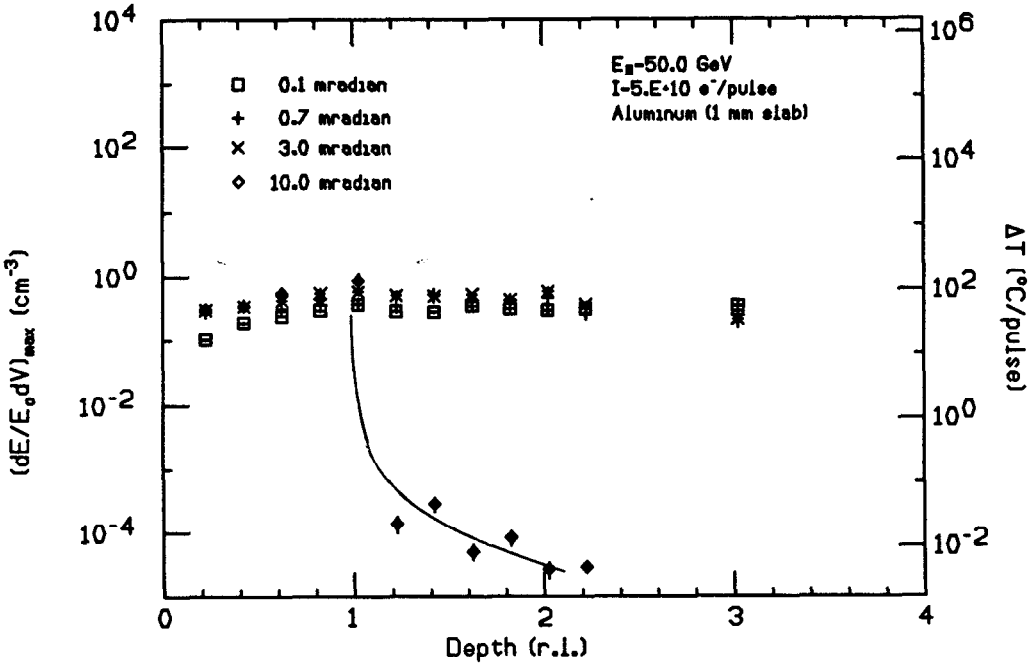

The maximum temperature rise for 50μ beams of 5×10^{10} electrons per pulse was found to increase with angle, ranging from about

- 300 to 700 ° C/pulse for copper
- 50 to 100 ° C/pulse for aluminum

for angles of incidence between 0.1 and 10 mradians. The results would also be applicable to slabs thicker than 1 mm within this angular range. For larger angles where shower leakage out the back becomes appreciable, the slabs were made thicker and the results (12) are shown for aluminum in Fig. 7.

FIG.7: MAXIMUM TEMPERATURE RISE VERSUS SIN θ FOR ELECTRON BEAMS WITH σ=0.05 MM

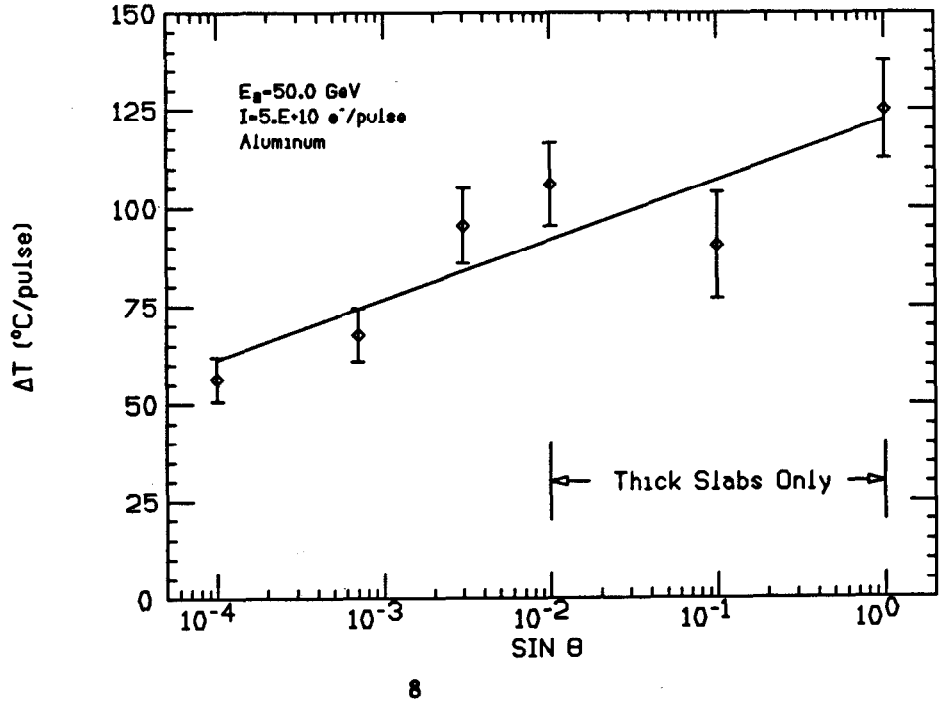

From these figures, accelerator designers were able to understand the nature of the temperature rises which could occur with small beam sizes. Fortunately, beams are as large or larger than 50μ for most of the linac and arcs, being focused smaller only in the final focus and interaction areas. Following the interaction region, the beams once again become blown up before reaching the beam dumps. Partially as a result of these calculations, the beam transport pipe for the SLC arcs has been made of aluminum rather than copper.

Beam Position Monitors

One problem encountered with beam position monitors (BPM) has been failure due to excessive heating, usually caused by beam missteering. To preclude this, BPM's for the SLC were designed to be shadowed such that the beam can never strike them. However, a beam striking the beam pipe or a flange upstream can initiate a shower with some fraction of the energy being deposited in the BPM downstream. Again, the amount and character of that energy was studied (13) with EGS4.

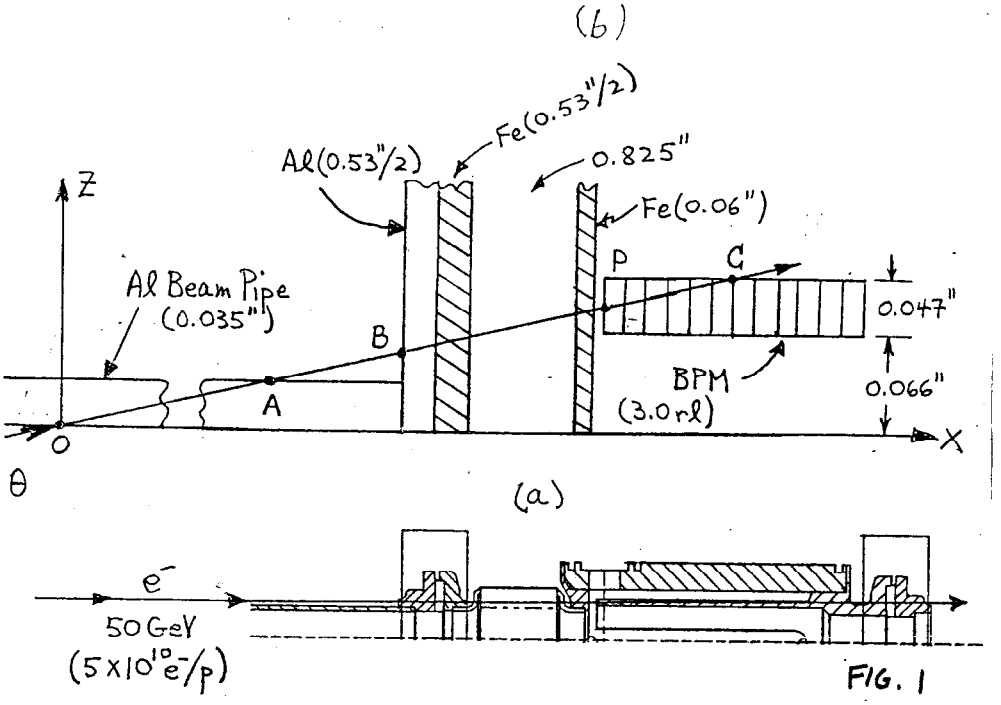

Figure 8. Cutaway view of the upper half of a BPM, beam pipe and flange (lower figure) with the EGS geometry representation shown above it.

Fig. 8 is a cutaway view of the upper half of a BPM along with the EGS representation showing the beam pipe, flanges, and a vacuum where the flexible bellows would

exist. In looking at this figure, we see some of the difficulties in trying to calculate analytically the energy deposition in the BPM. First, on the average the core of the shower will follow the straight line beam direction. Thus, the beam must be pointing toward the BPM in order to deposit substantial amounts of energy, and even then the stochiastic nature of shower events occurring upstream might prevent it from happening on an event-by-event basis. Second, if the angle is shallow (*i.e.*, a few milliradians), the beam traverses more aluminum beam pipe before reaching the BPM. This also places the beam entrance point further from the BPM. When multiple scattering and other processes are considered, it is virtually impossible to predict analytically exactly what the shower will look like when it reaches the BPM.

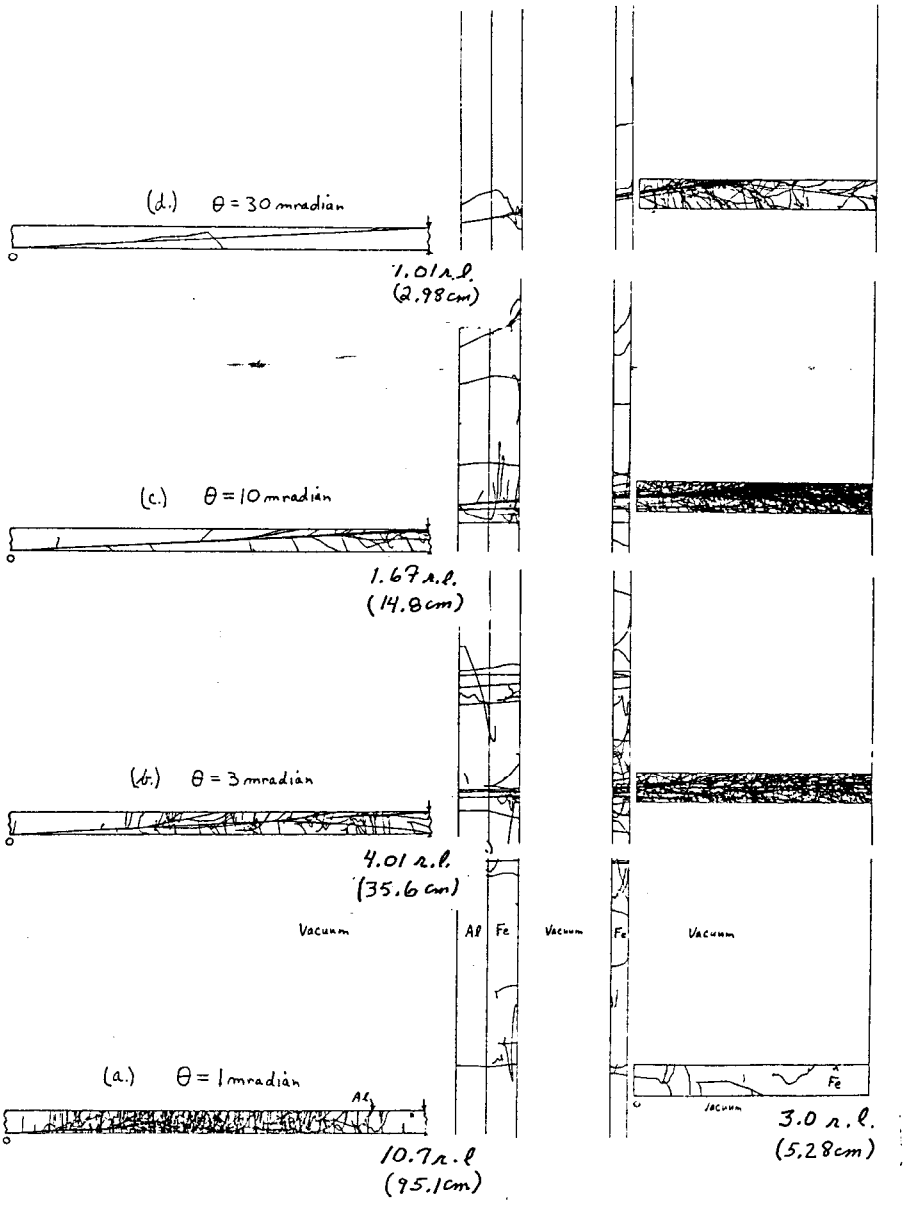

Figure 9. Shower events from a single 50 GeV electron at four different angles.

Fig. 9 shows what happens in an iron BPM downstream from a single 50 GeV electron incident upon an aluminum beam pipe for four different angles of incidence. In this EGS representation, only charged particles are shown, and only in the material of the the beam pipe, flanges and BPM. Fig. 10 shows the same thing but for a single angle of incidence. In both views, the beam is incident upon an aluminum pipe. In the upper half

of Fig. 10, the BPM is made of iron. In the lower figure, the material of the BPM is aluminum. That change is responsible for the lower energy deposition.

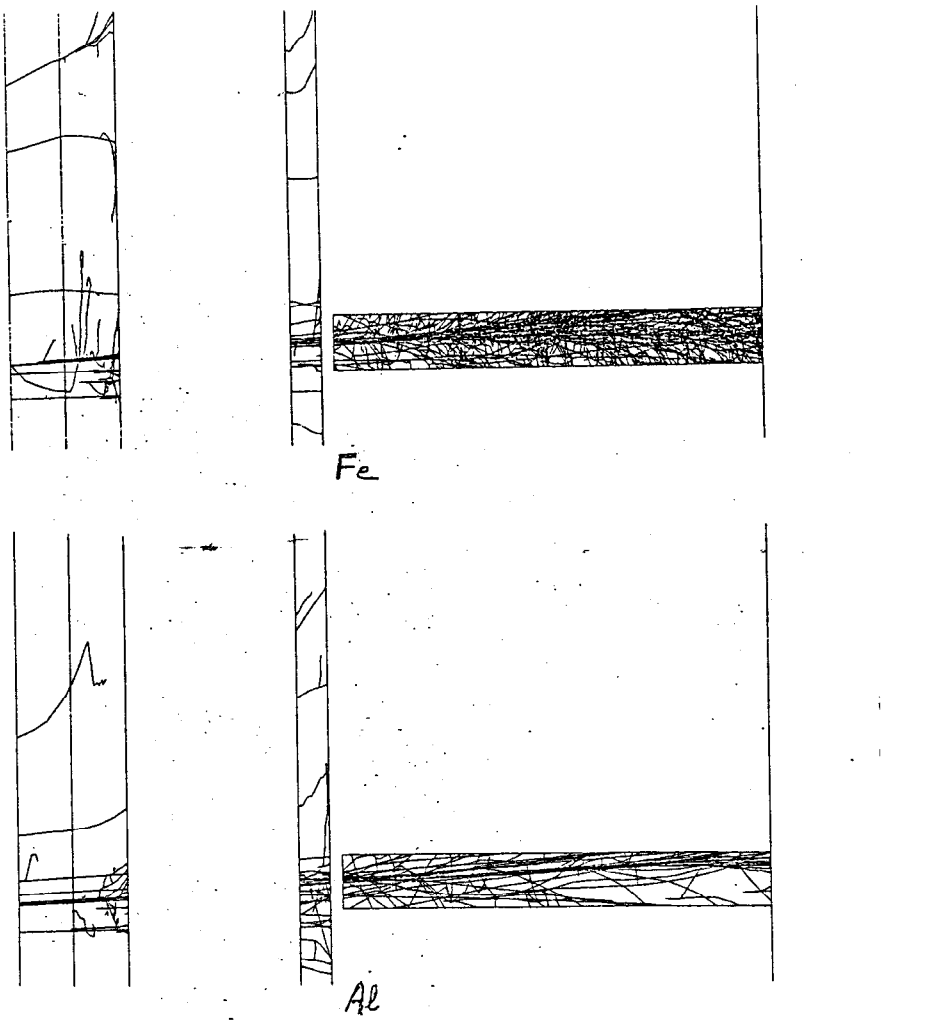

Figure 10. Shower events from a single 50 GeV electron incident at 3 mrad on an aluminum beam pipe (not shown), with either an iron BPM (a) or an aluminum BPM (b).

Corresponding to these unusually visual pictures, plots of the temperature rise as a function of the angle of incidence, for both iron and aluminum BPM's, are shown in Fig. 11 for a Gaussian input beam ($\sigma = 50\mu$) with energy of 50 GeV (13). The fraction of the input energy that is actually deposited in the BPM (either iron or aluminum) as a function of the angle of incidence is shown in Fig. 12.

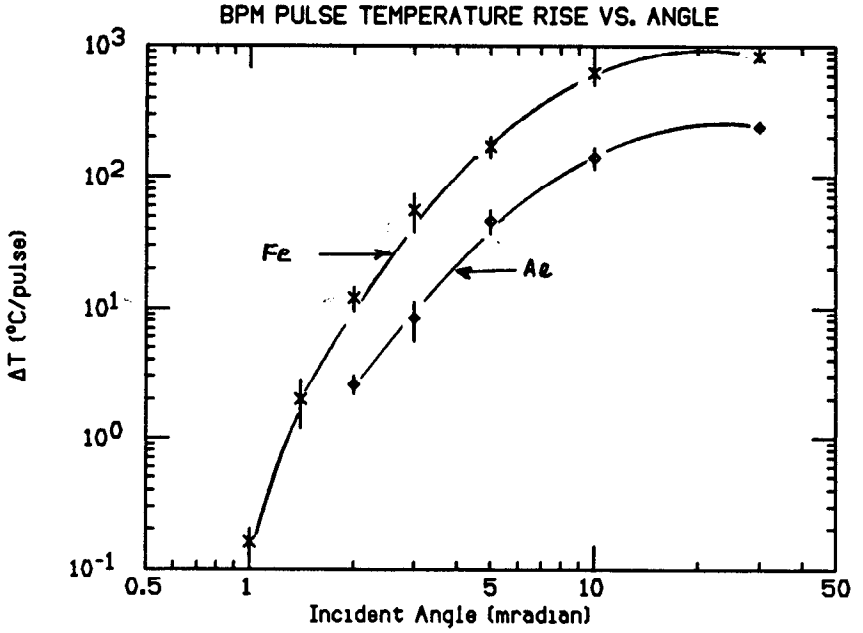

Figure 11. BPM pulse temperature vs angle.

Fig. 11 gives the BPM temperature rise versus angle for iron and aluminum.

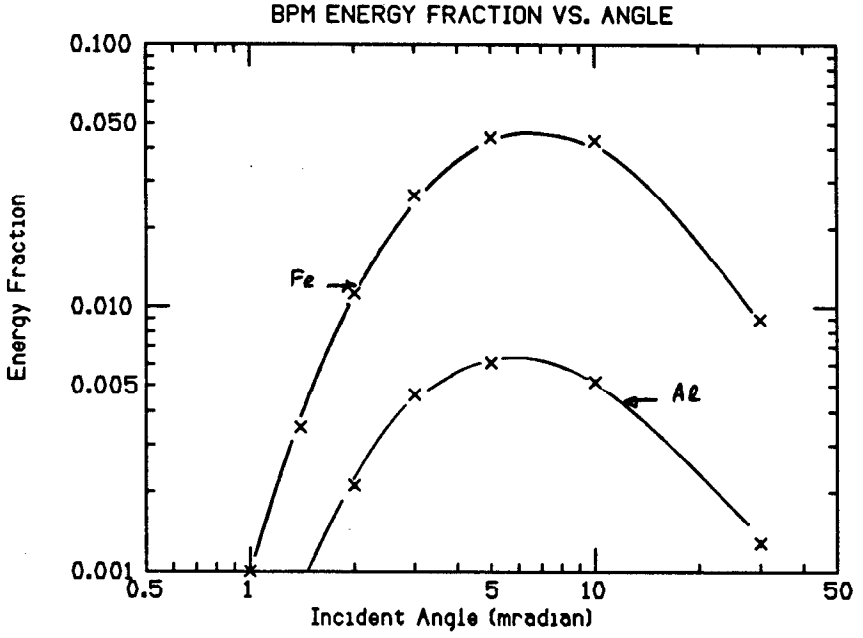

Figure 12. BPM energy fraction vs angle for iron and aluminum.

As a result of these studies, the BPM's were constructed of aluminum.

Lambertsen Magnet

The Lambertsen magnet associated with the positron target will have high current, high density beams near the poles of the magnet. To protect the magnet from damage, a spoiler (*i.e.*, scattering foil) may need to be placed upstream to protect against any mis-steered beams. The spoiler must be thick enough to blow up the beam through multiple scattering such that heating is within tolerable levels. There was concern, however, that since most of the beam energy is converted into bremsstrahlung ($\approx 63\%$ in 1 X_0), and the

angular spread of bremsstrahlung is some 28 times less than the spread of the electron beam due to multiple scattering, the temperature rise could still be too great due to the photon-initiated shower.

To be more explicit, the Gaussian width for electrons due to multiple scattering is

$$\theta_{MS} = \frac{14.1\sqrt{t}}{E_0},$$

and for photons the characteristic angle for bremsstrahlung is $\theta_{brem} \simeq \frac{m}{E_0}$.

Therefore, for a 1 X_0 target,

$$\frac{\theta_{brem}}{\theta_{MS}} = \frac{m}{14.1} = \frac{1}{28}.$$

The temperature rise is essentially proportional to energy which is inversely proportional to area. Thus, with the ratio of areas proportional to θ^2, we have

$$\left(\frac{\theta_{brem}}{\theta_{MS}}\right)^2 = \left(\frac{28}{1}\right)^2 \simeq 800.$$

That is, the energy density from the bremsstrahlung could result in very high temperatures in the magnet, perhaps as much as 500 times ($0.63 \times 800 = 500$) greater than multiply scattered electrons, and an EGS4 simulation seemed called for.

Fig. 13 gives the maximum temperature rise for both spoiler and magnet as a function of spoiler thickness as calculated by EGS (14). Separation distances between spoiler and magnet of 50 and 100 cm are shown in this figure. From this we see that temperature rises in both spoiler and magnet iron of less than 100^oC /pulse are possible for 100μ (Gaussian σ) beams and 5×10^{10} electrons of 33 GeV per pulse.

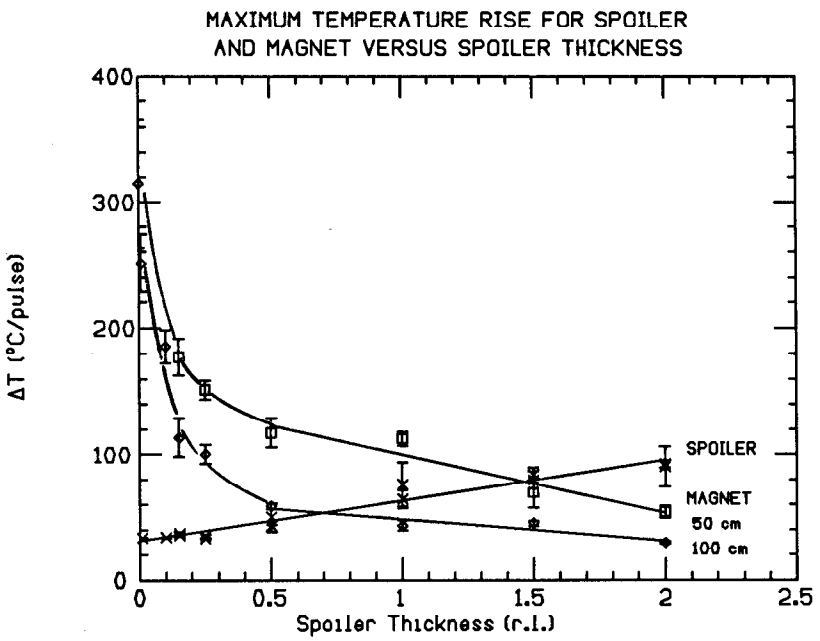

Figure 13. Maximum temperature rise for spoiler and magnet versus spoiler thickness.

From a study of the EGS results, the apparent reason why the energy deposition from bremsstrahlung isn't as great as one might expect is seen to be due to the *multiple scattering of the electrons before the bremsstrahlung is produced.*

PANOFSKY LONG ION CHAMBER RESPONSE

Some sort of detector is needed in the SLC arcs to provide information on the magnitude and location of beam losses. Two Panofsky Long Ion Chambers (15), called PLIC's, will be installed along each arc, one on each side of the magnet string. A similar system, but with a single, larger PLIC, has been in use at SLAC for 20 years. Measurements were made on the original PLIC by steering a 7 GeV electron beam into a section of the SLAC accelerator with a 2 volt signal observed for a 10 kW beam loss (16). The requirements for the SLC PLIC will be for a 720 W beam loss to give a signal large enough to shut off the beam.

We would like to understand exactly what caused the signal in the linac ion chamber experiment (16) — what was the spectrum emerging from the beam pipe and impinging upon the ion chamber, how much of the beam pipe was involved and what components of the ion chamber are important in making up the signal (*i.e.*, how is the energy deposited in the ion chamber gas). With this knowledge, EGS can then be used with confidence to predict the absolute magnitude of a PLIC signal from a given amount of beam loss in the SLC arcs.

Some of the differences between the linac and SLC PLIC's are 1) the diameter of the SLC PLIC is only about 1/3 of the diameter of the PLIC used in the linac, 2) the SLC PLIC will be close to the arc magnets (about 16 cm) whereas the one in the linac is about 2 meters away from the beam, and 3) the linac beam pipe is radically different from that of the SLC arcs.

With these differences in mind, EGS4 was first run (17) for the linac geometry using a full cylindrical geometry mockup of the wave guide, and the results are given in Table 2. An accelerator length of 30 meters was used, with the radiation emanating from the waveguide scored at a radial distance of 200 cm, corresponding to the actual location of the PLIC in the SLAC tunnel. The first result was that essentially all of the signal is induced within a distance of about 15 meters measured from the shower origin, consistent with the measurements (16). The energy distribution of the photons and the charged particles was also scored, and the average energy found to be about 1 MeV for photons and 10 MeV for charged particles. Almost all of the energy reaching the accelerator PLIC is accounted for by photons (*i.e.*, $15.0\%(\gamma) + 1.2\%(e^{\pm}) = 16.2\%$).

Table 2

Radiation Component	Wave Guide Leakage	Deposition in Insulation-Wall	Deposition in Argon Gas	Discard Region	Conversion Efficiency
γ	15.0%	1.60%	3.81%	9.60%	$\alpha_\gamma = 3.81/15.0 = 0.254$
$e^{\pm}$	1.20%	0.470%	0.390%	0.340%	$\alpha_e = 0.390/1.20 = 0.325$
$\gamma + e^{\pm}$	16.2%	2.10%	4.20%	9.90%	$\alpha_\gamma + \alpha_e = 0.579$

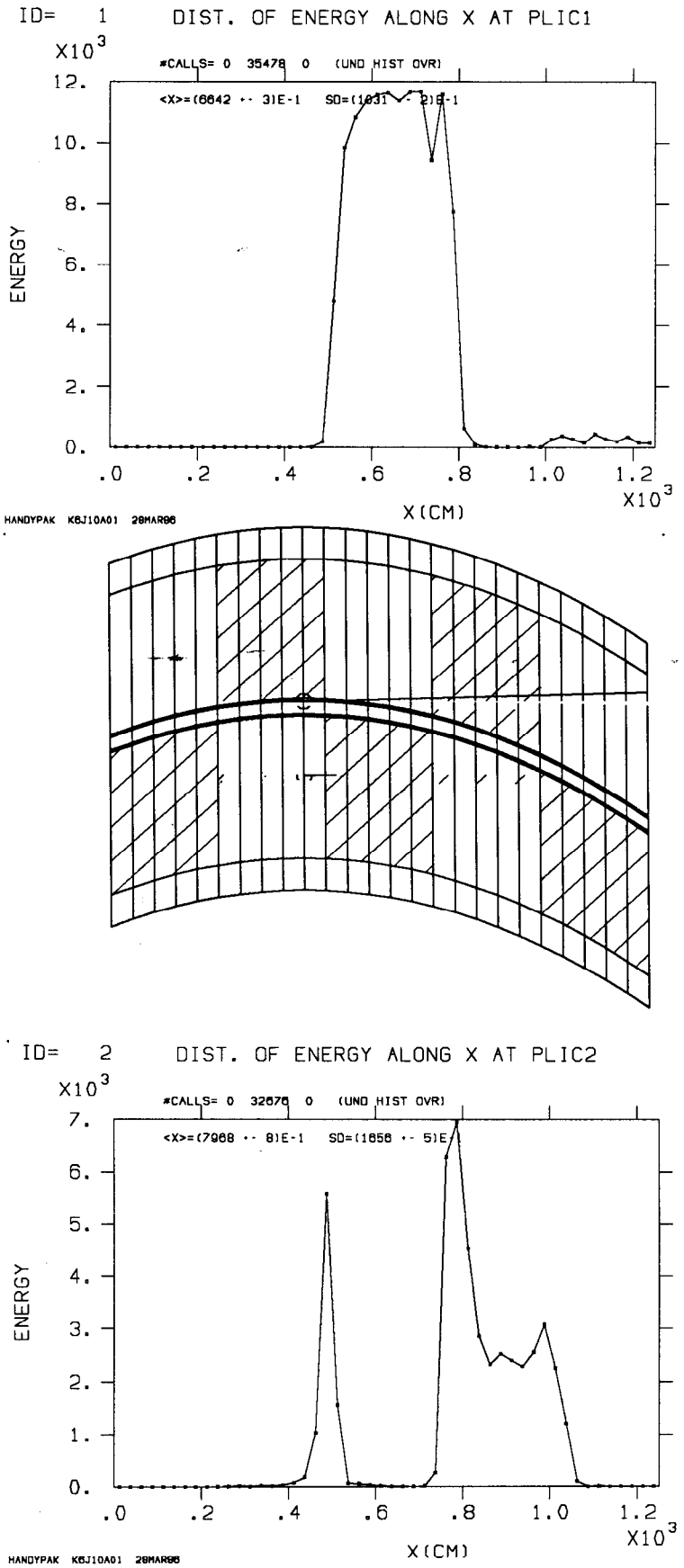

Fig. 14. Energy reaching surfaces of PLIC1 and PLIC2.

With some understanding of the linac measurements and the EGS linac simulation, we could turn to an EGS simulation of the SLC arcs, the geometry of which is shown in the middle of Fig. 14. In this figure the beam pipe is represented by the dark curved lines (actually, a pair of two closely spaced lines) that extend from left to right along the general direction of the beam. The figure is purposely distorted such that the total horizontal distance represents 1250 cm, whereas the vertical distance covers about 16 cm on either side of the beam pipe. The cross-hatched areas represent magnet iron and the beam pipe material is aluminum. The rest of the regions in this geometry, including the center of the beam pipe, are vacuum. This slab geometry is semi-infinite—*i.e.*, the slabs extend forever into and out of the plane of the paper.

The curvature of the SLC arcs was approximated by rotating the "horizontal" sides of each slab by a slight amount while keeping the vertical sides of all slabs parallel to one another. The amount of curvature applied at each point of rotation was chosen such that the beam moved a distance of 1 cm after having traveled a distance of 250 cm (*i.e.*, the distance associated with each of the *five* magnets depicted by the cross-hatching). It should be pointed out, however, that the overall results were not greatly affected by the addition of curvature to the geometry.

In this figure, the circle and ray indicate the location and direction, respectively, of an incident beam impinging upon the SLC beam pipe at a 1 mradian angle relative to the surface of the particular slab at that position. The curved lines at the very top and bottom of the figure designate the locations of the *two* PLIC cables, PLIC1 and PLIC2, respectively, that will be positioned 16 cm from the beam centerline.

The resultant EGS simulation of this geometry first tells us that the average energy of the photon radiation reaching either PLIC is 1 to 2 MeV, whereas the average charged particle energy is 10 to 20 MeV, more-or-less in agreement with the linac spectra.

In order to determine if there is a situation in which the shower leakage is effectively "hidden" from either or both PLICs, a series of calculations was done for incident beam positions varying from 50 cm to 550 cm, and for beams directed toward and away from PLIC1. The results of all the EGS4 calculations for the SLC arcs are summarized in Table 3.

The energy percentage seen by an individual PLIC ranges from 2 to 20%. The sum, however, only varies from 12 to 22% because when one PLIC becomes "hidden" the other becomes "visible". This leads to voltages in the 2-10 volt range.

Using the data from Table 3, the PLIC signal voltages (PLIC1 + PLIC2) are plotted in Fig. 15 as a function of the location of the incident beam along the magnet structure for the two beam directions (toward PLIC1 or toward PLIC2).

Table 3. Summary of EGS4 calculations for SLC PLICs.

Run ID	Beam Location (cm)	Beam Direction	Radiation Component	PLIC1	PLIC2	PLIC1 + PLIC2
K6J2A01	50	Toward PLIC1	γ	2.07	3.86	5.93
			$e^{\pm}$	6.06	1.95	8.01
			$\gamma + e^{\pm}$	8.13	5.81	13.94
K6J4A01	150	Toward PLIC1	γ	1.32	6.22	7.54
			$e^{\pm}$	2.22	6.18	8.40
			$\gamma + e^{\pm}$	3.54	12.40	15.94
K6J6A01	250	Toward PLIC1	γ	0.87	6.75	7.62
			$e^{\pm}$	1.13	13.55	14.68
			$\gamma + e^{\pm}$	2.00	20.30	22.30
K6J8A01	350	Toward PLIC1	γ	1.80	4.38	6.18
			$e^{\pm}$	2.37	8.16	10.53
			$\gamma + e^{\pm}$	4.17	12.54	16.71
K6J10A01	450	Toward PLIC1	γ	3.69	2.29	5.98
			$e^{\pm}$	6.09	1.43	7.52
			$\gamma + e^{\pm}$	9.78	3.72	13.50
K6J12A01	550	Toward PLIC1	γ	2.07	3.53	5.60
			$e^{\pm}$	6.08	1.65	7.73
			$\gamma + e^{\pm}$	8.15	5.18	13.33
K4J2A01	50	Toward PLIC2	γ	2.32	5.33	7.65
			$e^{\pm}$	4.79	8.19	12.98
			$\gamma + e^{\pm}$	7.11	13.52	20.63
K4J4A01	150	Toward PLIC2	γ	1.71	4.16	5.87
			$e^{\pm}$	2.53	6.57	9.10
			$\gamma + e^{\pm}$	4.24	10.73	14.97
K4J6A01	250	Toward PLIC2	γ	2.08	3.23	5.31
			$e^{\pm}$	2.24	7.22	9.46
			$\gamma + e^{\pm}$	4.32	10.45	14.77
K4J8A01	350	Toward PLIC2	γ	2.01	3.58	5.59
			$e^{\pm}$	2.90	2.55	5.45
			$\gamma + e^{\pm}$	4.91	6.13	11.04
K4J10A01	450	Toward PLIC2	γ	2.84	5.79	8.63
			$e^{\pm}$	5.74	5.87	11.61
			$\gamma + e^{\pm}$	8.58	11.66	20.24
K4J12A01	550	Toward PLIC2	γ	2.14	5.54	7.78
			$e^{\pm}$	4.75	8.44	13.19
			$\gamma + e^{\pm}$	6.89	13.98	20.87

Note: The numbers above give the percentage of the total incident energy reaching one or both PLICs.

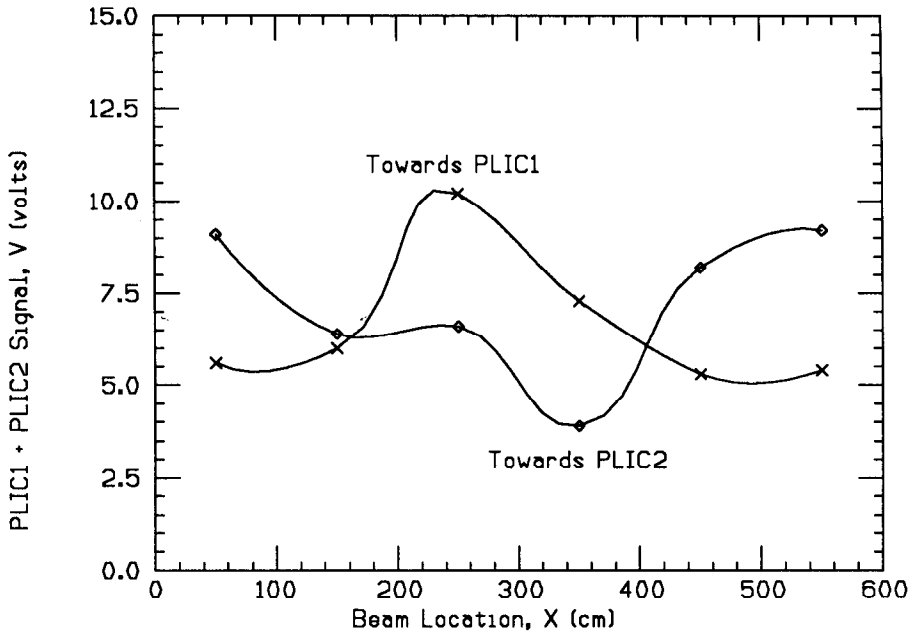

Figure 15. PLIC1 + PLIC2 signal vs. incident beam location.

The voltages, which range from 3 to 10 volts, are higher than the 1-2 volt numbers calculated previously with a simple model. However, the magnetic field associated with the SLC arc was not taken into account in any of the calculations presented in this study. Under the extreme condition where none of the charged particles reach the PLIC, the signal voltage would only be 0.25 to 0.36 volts. A more reasonable guess may be that all the photon and half the charged particle energy indicated in Table 3 will contribute to the signal. Applying this, the SLC PLIC signals should be in the range of 2 to 5 volts.

RADIATION DAMAGE TO ELECTRONICS IN THE ARC ALCOVES.

The arcs originally were envisaged as radiation-free areas, with essentially no beam losses. This is still the case for most of the arcs, but not the final focus, which includes about 600 feet on either side of the interaction point. In this region, the beam will be intercepted by collimators both before it reaches the interaction point (IP) and after as it travels to the beam dump. There are three alcoves on each side of the IP in the final focus areas which contain sensitive electronics. There are 14 other such alcoves in the arcs leading to the final focus.

For the first 14 alcoves, the only source of radiation comes from synchrotron radiation (18). The critical energy of the synchrotron radiation from a 50 GeV electron beam in these arcs is about 950 keV; after large angle scattering in the beam pipe, the energy of the escaping radiation will be about 330 keV.

EGS4 was run on the geometry of the arcs to determine the fraction of synchrotron energy that escapes from the beam pipe-magnet structure into the tunnel, and to calculate the absorbed dose to silicon at a distance of 1 meter. The results were that about 23% of the energy escapes the beam pipe from the outer wall (*i.e.*, where the synchrotron radiation is striking) and about 21% from the inner wall (the side opposite where the radiation initially strikes). For a beam energy of 50 GeV, the annual dose to silicon will be about 5×10^4 rads per year.

In the final focus area however, beam losses rather than synchrotron radiation are the problem (19). Here, we have been fortunate in that the beam transport codes have been improved to where beam losses *in each device* are available. These are given in Table 4.

Table 4
Devices and Beam Losses

Device	Distance From IP (m)	$e^{\pm}$/pulse South		$e^{\pm}$/pulse North	
		Incoming	Outgoing	Incoming	Outgoing
Dump	167.1 (S)	5×10^{10}		–	
Dump	183.6 (N)	–		5×10^{10}	
TD-23	146.4	5×10^{10}		5×10^{10}	
PC-24	148.0	–	–	1.7 +4	–
C0	142.2	4.9 +7	–	4.0 +4	–
PC-19	134.9	–	–	4.5 +2	–
PC-18	124.1	8.2 +6	1.0 +6	6.7 +3	5.5 +9
C1X	114.0	2.6 +8	–	2.5 +8	1.6 +5
C1Y	112.0	3.1 +8	7.1 +8	1.4 +8	4.0 +7
PC-16.5	108.5	–	–	3.6 +2	1.3 +5
PCB-3	100.4	–	–	–	1.4 +7
PC-14	95.7	–	6.6 +7	1.4 +3	2.7 +7
PC-12.5	86.7	–	–	–	9.6 +5
PC-12	81.0	2.1 +7	2.0 +7	2.9 +7	4.0 +8
PC-11.5	77.0	5.8 +2	9.4 +7	2.1 +3	–
PC-10.5	71.9	8.4 +7	1.3 +9	3.7 +7	8.2 +7
PC-10	65.5	5.6 +6	9.8 +8	5.5 +6	9.6 +7
PC-8.5	56.5	–	–	–	1.0 +5
PC-8	50.6	1.1 +7	2.4 +8	3.9 +7	3.8 +8
PC-7.5	46.8	3.0 +7	4.4 +8	–	6.8 +2
ST-4	19.8	5.0 +10	–	5.0 +10	–

(Note: Read 5.0 +10 as 5.0×10^{10}.)

Information such as is given in Table 4 would have been unheard of ten years ago to the health physicist; it is a powerful tool (assuming its accuracy) and one which should be more and more available in the future.

The three types of devices which will be sources of radiation to the final focus alcoves are 1) the main dumps (which absorb 72 kW continuously), 2) the tune-up dumps (two per final focus) which will be inserted in the beam line for only a few hours each day, and 3) collimators (particularly adjustable ones). Doses from these devices will come mostly from bremsstrahlung radiation and from giant resonance neutrons. Table 5 summarizes the annual doses in the final focus alcoves.

Table 5

Annual Photon Doses and Neutron Fluences.

Alcove	γ (rad/yr)	Neutron $(n - cm^{-2} - yr^{-1}$
S-15	4.6 +5	6.7 +12
S-15T	4.5 +6	1.2 +14
S-16	1.0 +6	5.0 +13
N-14	1.0 +4	1.7 +11
N-15	1.8 +6	5.8 +13
N-15T	2.8 +5	1.3 +13
N-16	6.8 +4	1.2 +12

(Note: Read 4.6 +5 as 4.6×10^5.)

The conclusions from these studies are that without extra shielding, many of the electronic components will begin to fail within a few hours, and that some combination of local shielding around the sources and the alcoves themselves will be necessary if the electronics are to remain in the tunnels.

Concluding Remarks

The radiation transport problems associated with the design of the SLC, while diverse and unique, have lent themselves to solutions using a combination of sophisticated Monte Carlo codes and analytic-empirical methods. EGS4 is particularly well suited for these types of problems, but other codes such as MORSE for low energy neutron transmission, have also proved very helpful.

Acknowledgements

Almost the entire SLAC staff has in some way been involved in the design and construction of the SLC upon which this note is based. We are particularly grateful to those working on the SLC without whose input this work would have been impossible; among them are G. Fischer, S. Ecklund, H. DeStaebler, Jr., W. Kozanecki, and R. Larsen. Also, we wish to acknowledge the input and suggestions of R. C. McCall and other members of the Radiation Physics group at SLAC.

References

1 See, for example, G.E. Fischer (for the SLAC Staff), "SLC— Status and Development", SLAC PUB-4012 (1986).

2. W.P. Swanson, "Radiological Safety Aspects of the Operation of Electron Linear Accelerators", IAEA Tech. Report 188 (1979).

3. NCRP, "Radiation Protection Design Guidelines for 0.1-100 MeV Particle Accelerator Facilities," NCRP Report 51 (1977).

4. H. DeStaebler, T. M. Jenkins, and W. R. Nelson, "Shielding and Dosimetry", Chapter 26 in THE STANFORD TWO-MILE ACCELERATOR edited by R. B. Neal (W. A. Benjamin, Inc., New York, 1968).

5. H. DeStaebler, Jr., "Transverse Radiation Shielding for the Stanford Two-Mile Accelerator", SLAC Report SLAC-9 (1962).

6. T.M.Jenkins, "Neutron and Photon Measurements Through Concrete from a 15 GeV Electron Beam on a Target - Comparison with Models and Calculations", Nucl. Inst. Meth. 159 p. 265 (1979).

7. A. Van Ginneken, "CASIM. Program to Simulate Hadronic Cascades in Bulk Matter", Fermilab Report Number FN-272 (1975); see also A. Van Ginneken, "Calculation of the Average Properties of Hadronic Cascades at High Energies (CASIM)", Chapter 21 in COMPUTER TECHNIQUES IN RADIATION TRANSPORT AND DOSIMETRY, edited by W. R. Nelson and T. M. Jenkins (Plenum Press, New York, 1980).

8. R.L Ford and W.R. Nelson, "The EGS Code System: Computer Programs for the Monte Carlo Simulation of Electromagnetic Cascade Showers (Version 3)", SLAC Report Number SLAC-210 (1978).

9. P. A. Aarnio, J. Ranft and G. R. Stevenson, "A Long Writeup of the FLUKA82 Program", CERN Divisional Report Number TIS-RP/106 Rev (1984).

10. S. Ecklund and W. R. Nelson, "Energy Deposition and Thermal Heating in Materials Due to Low Emittance Electron Beams", SLAC Note CN-135 (1981).

11. W.R. Nelson, H. Hirayama and D.W.O. Rogers, "The EGS4 Code System", SLAC Report Number SLAC-265 (1985).

12. W. R. Nelson and T. M. Jenkins, "Temperature Rise Calculations for the Beam Pipe in the SLC Arcs", SLAC Note CN-235 (1983).

13. W. R. Nelson and T. M. Jenkins, "Temperature Rise in Iron Beam Position Monitors", SLAC Note CN-275 (1984); see also W. R. Nelson and T. M. Jenkins, "Temperature Rise in Aluminumm Beam Position Monitors", SLAC Note CN-276 (1984).

14. W. R. Nelson and T. M. Jenkins, "Temperature Rise in the Lambertsen Septum Magnet Associated with the Positron Target", SLAC Note CN-262 (1984).

15. W.H.K. Panofsky, ""The Use of a Long Co-axial Ion Chamber Along the Accelerator", SLAC Note TN-63-57 (1963).

16. M.G. Kendall and D. Reagan, IEEE Trans. Nul. Sci. NS-14, No. 3, p.1096 (1967).

17. T. M. Jenkins, W. R. Nelson and D. D. Reagan, "PLIC Signal Voltages in the SLAC Accelerator Scaled to the SLC Arcs", SLAC Note CN-331 (1986). 1968).

18. T. M. Jenkins and W. R. Nelson, "Synchrotron Radiation in the Collider Arcs", SLAC Note CN-69 (1981).

19. T. M. Jenkins and R. C. McCall, "Radiation in the SLC Final Focus Alcoves from Beam Loss in Collimators and Dumps", SLAC Note CN-337 Rev. (1986).

20. T. W. Armstrong and K. C. Chandler, "HETC — A High Energy Transport Code", Nucl. Sci. and Eng. 49, p. 110 (1972).